Bull. Mater. Sci., Vol. 20, No. 2, April 1997, pp. 265–277. © Printed in India.

A comparative study on the processing, dielectric and electrical properties of PMN based solid solutions

KAMAL SINGH* and SHEELA BAND†
Department of Physics, Amravati University, Amravati 444 602, India
†Department of Applied Physics, Y. C. Engineering College, Wanadongari 441 110, India

MS received 9 April 1996; revised 13 November 1996

Abstract. Lead magnesium niobate (PMN) based binary with lead titanate (PT), lead iron niobate (PFN) and lead zinc niobate (PZN) and ternary with PZN–PT and PFN–PT solid solutions have been synthesized. In depth characterization using X-ray diffraction and SEM techniques have revealed the major perovskite phase formation. Amongst all the solid solutions, PMN–PZN–PT has given the highest values of permittivity as 19,740 and 23,700 with T_c as 34°C when sintered at 1080°C and 1180°C respectively on the one hand and on the other, PFN containing solid solutions exhibited distinct deviation from the relaxor behaviour.

Keywords. Solid solution; sintering; relaxor; microstructure.

1. Introduction

In the late 1950s Smolenskii and Agranovskaya (1959), discovered a family of lead based perovskites with general formula $A(B' B'')O_3$ exhibiting diffuse phase transition (DPT). Many of these DPT materials are relaxors offering very high relative permittivity in the range 8000–25,000 which have been of a great commercial importance due to their applications in multilayer capacitors, electrostatic actuators, pyroelectric detectors, bolometers etc.

Amongst the lead based relaxors, PMN and PZN have exhibited high relative permittivity (14,000–20,000) (Swartz *et al* 1984; Lejeune and Boilot 1985; Wang and Schulze 1990; Singh and Band 1996) and 22,000 (Bokov and Mylnikova 1961) respectively. But PMN has been most widely studied as compared to PZN owing to relative ease of preparation as the latter was found to be extremely difficult to obtain in the pure perovskite ceramic form by conventional mixed oxide method or as suggested by Swartz and Shrout (1982). The ferroelectric transition T_c of PMN below room temperature (-8 to -15°C) has been one of the factors which constraints its practical utilization.

Several authors have shown that the substitutional effect of PT in PMN resulted in the rise in permittivity, shift of T_c towards room temperature and also an improvement in the extent of perovskite phase formation (Swartz *et al* 1984; Yan *et al* 1989; Bouquin and Lejeune 1991; Ravindranathan *et al* 1991). Landin and Schulze (1990) observed rapid densification in case of 0·7 PMN–0·3 PZN solid solution at 1100°C. Furthermore, in this system, the maximum permittivity at 20°C has also been obtained. Desgardin *et al* (1983), in their investigation on ceramic compositions based on PMN have obtained T_c around 20°C for a particular composition 0·77 PMN–0·23 PFN. In addition to this, the use of selective flux therein offered them weak dielectric loss and high resistivity.

*Author for correspondence

Table 1. Composition and designation of PMN based solid solutions.

Composition	Constituents	Sintering temperature (°C)	Designation
		1080	PMT1
0·9PMN–0·1PT	PbO, MN, TiO_2		
		1180	PMT2
		1080	PMZN1
0·7PMN–0·3PZN	PbO, MN, ZN		
		1180	PMZN2
		1080	PMFN1
0·7PMN–0·3PFN	PbO, MN, FN		
		1180	PMFN2
		1080	PMZNT1
0·85PMN–0·07PZN–0·08PT	PbO, MN, ZN, TiO_2		
		1180	PMZNT2
		1080	PMFNT1
0·85PMN–0·07PFN–0·08PT	PbO, MN, FN, TiO_2		
		1180	PMFNT2

Eventhough there have been several reports on the investigations of PMN based solid solutions but still a comparative study on the sintering temperature, grain size, relative permittivity, low losses, electrical resistivity and T_c nearing room temperature in the summarized form is of importance. Hence, in the present study we have made an attempt to undertake a comparative study on the processing of PMN based binary and ternary solid solutions such as PMN–PT, PMN–PZN, PMN–PFN, PMN–PZN–PT and PMN–PFN–PT following a structural characterization, dielectric and electrical properties with a focus on the microstructures.

2. Experimental

Ceramics of the selected compositions shown in table 1 have been synthesized using Swartz's technique (Swartz and Shrout 1982). The initial ingradients PbO, MgO, ZnO, Nb_2O_5, Fe_2O_3 and TiO_2 used have been of 99·9%. Initially, the coulumbites $MgNb_2O_6$ and $ZnNb_2O_6$ have been prepared by taking $MgO:Nb_2O_5$ in 1·02:1 and $ZnO:Nb_2O_5$ in 1:1 molar ratios, followed by calcination and re-calcination at 1000°C for 4 and 2 h respectively. Later wolframite $FeNbO_4$ has been prepared by taking Fe_2O_3 and Nb_2O_5 in 1:1 molar ratio and calcining for 4 h at 1000°C. Thus prepared $MgNb_2O_6$, $ZnNb_2O_6$ and $FeNbO_4$ have been designated as MN, ZN and FN respectively. Finally the solid solutions of above mentioned compositions have been prepared by taking presynthesized constituent oxides in appropriate molar ratios followed by a number of processing steps as shown in figure 1. In order to overcome PbO losses, the pellets have been surrounded by the powder of the same composition. Various ceramics prepared have been designated as given in table 1. The bulk densities of sintered pellets have been measured using Archimedes principle.

X-ray diffractometer (XRD) scans have been recorded on powder of sintered pellets with the help of PW1700 X-ray powder diffractometer using iron target ($\lambda = 1{\cdot}93735$ Å) at the scanning rate of $2\theta = 2{\cdot}4°$/min at RSIC, Nagpur. The fractured surface of the

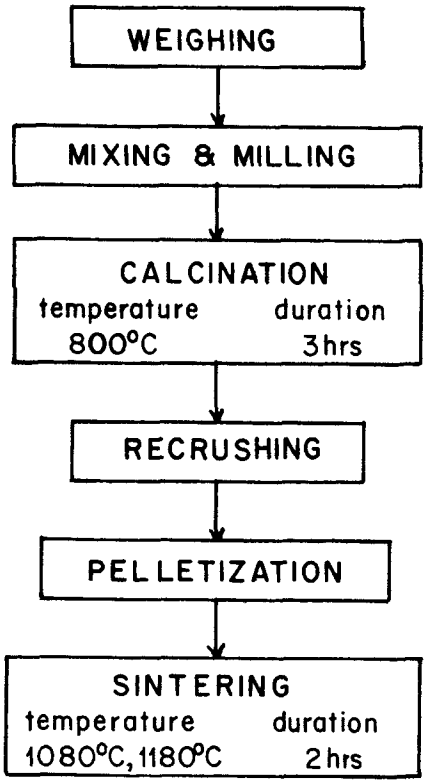

Figure 1. Flowchart of material processing of PMN based solid solutions.

sintered pellets has been examined by using Cambridge 250 Mark (III) scanning electron microscope (SEM) at RSIC, Nagpur.

The relative permittivity (ε) and dissipation factor ($\tan\delta$) have been measured using HP 4192A LF impedance analyser, pseudo-continuously in the frequency range from 0·1 to 100 kHz and temperature ranging from -50 to 100°C. The dc resistivity at room temperature has been measured using Keithley 617 programmable electrometer with an electric field 150 V/cm being applied across the samples.

3. Results and discussion

3.1 *XRD and SEM characterization*

The XRD patterns of PMT2, PMZN2, PMZNT2, PMFN2 and PMFNT2 are shown in figure 2. An excellent agreement between experimental 'd' values with standard JCPDS (File 27–1199) ones corresponding to PMN confirms perovskite phase formation. A critical analysis of XRD data reveals cubic symmetry of the perovskite phase in all samples. The relative % of perovskite phase formation is estimated using (1) below (Swartz and Shrout 1982; Wang and Schulze 1990; Singh and Band 1996),

$$\% \text{ perovskite} = \frac{\text{Iperov (110)}}{\text{Iperov (110)} + \text{Ipyro (222)}}, \tag{1}$$

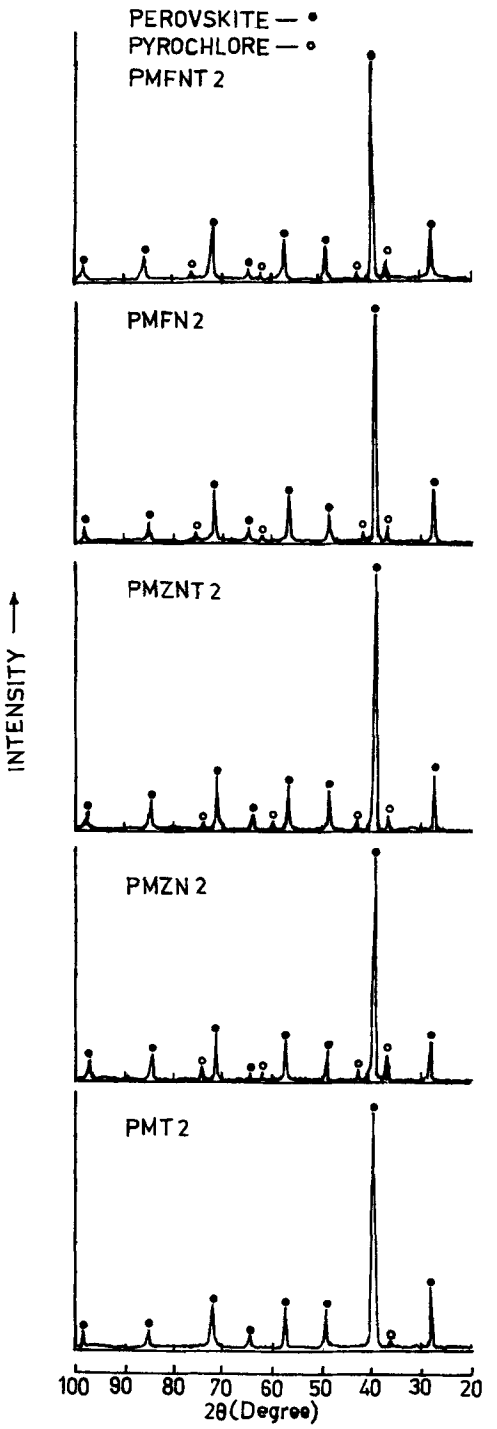

Figure 2. X-ray powder diffraction patterns of PMT2, PMZN2, PMZNT2, PMFN2 and PMFNT2.

Table 2. Perovskite phase (%) and lattice cell constant *a* of PMN based solid solutions.

Sample	Perovskite (%)	Lattice constant (Å)
PMT1	96·5	4·041 ± 0·001
PMT2	98·5	4·041 ± 0·001
PMZN2	91·0	4·056 ± 0·001
PMFN1	92·0	4·042 ± 0·001
PMFN2	94·5	4·042 ± 0·001
PMZNT2	95·0	4·040 ± 0·001
PMFNT1	94·0	4·042 ± 0·001
PMFNT2	93·0	4·041 ± 0·001

where, Iperov and Ipyro are the intensities of (110) and (222) characteristic lines respectively.

The % of perovskite phase along with the lattice cell constant values determined from high angle reflections are given in table 2. In addition to the absence of characteristics lines corresponding to solute phase, the variation of lattice cell constant *a* from 4·039 ± 0·001 to 4·056 ± 0·001 ensures the solid solution formation in all compositions. A systematic correlation of lattice cell constant with composition can not be predicted precisely. However, a comparatively high lattice cell constant obtained for PMZN2, which contains high concentration of Zn (30 mole %), is due to larger radius of Zn (0·74 Å) replacing smaller Mg (0·65 Å) in the B-site of ABO_3 perovskite structure. Goldschmidt (1926) concluded that, for the perovskite structure formation, tolerance factor should be within 0·88 to 1·09. The large value of tolerance factor indicates higher stability of perovskite phase. The values of tolerance factor for the perovskite compounds reported by Shrout and Halliyal (1987), follow the PZN < PMN < PFN < PT sequence with respective values of 0·984, 0·99, 1·0, 1·02. In the present case, the improvement in the perovskite phase is observed as a result of increased tolerance factor of the corresponding binary solid solution (table 2). Interestingly, it is observed that the addition of PT to PMN as well as to PMN–PZN solid solution stabilizes the perovskite phase (table 2) which is in good agreement with earlier findings (Bouquin and Lejeune 1991; Ravindranathan *et al* 1991).

The microphotographs of PMT2, PMZN1, PMZN2, PMFN2, PMZNT2 and PMFNT2 are displayed in figures 3a–f respectively. The grain size calculated from microphotographs using ASTM intercept technique is presented in table 3. A close look at these microphotographs reveals almost a similar morphology of the grains of all the samples confirming the maximum perovskite phase formation supporting strongly the XRD results.

In some samples a few distinct grains of pyrochlore, the second phase, are clearly seen. Furthermore, as a general behaviour of lead based perovskites, in all compositions the increased grain size with increasing sintering temperature is observed. A comparatively large perovskite grains are observed for PMN–PZN and PMN–PFN binary solid solutions. The PMN–PT solid solution, whereas, exhibits relatively smaller grains. The decrease in grain size with PT addition is observed in both PMN–PZN and PMN–PFN binary solid solutions (table 3).

3.2 *Dielectric properties*

The ε_{max}, T_c, $\tan\delta_{max}$ and T $\tan\delta_{max}$ at 0·1, 1, 10 and 100 kHz of all the samples are presented in table 4. The temperature dependence of ε and $\tan\delta$ at 0·1, 1, 10 and 100 kHz of typical samples PMZNT2 and PMFN2 are shown in figures 4 and 5 respectively.

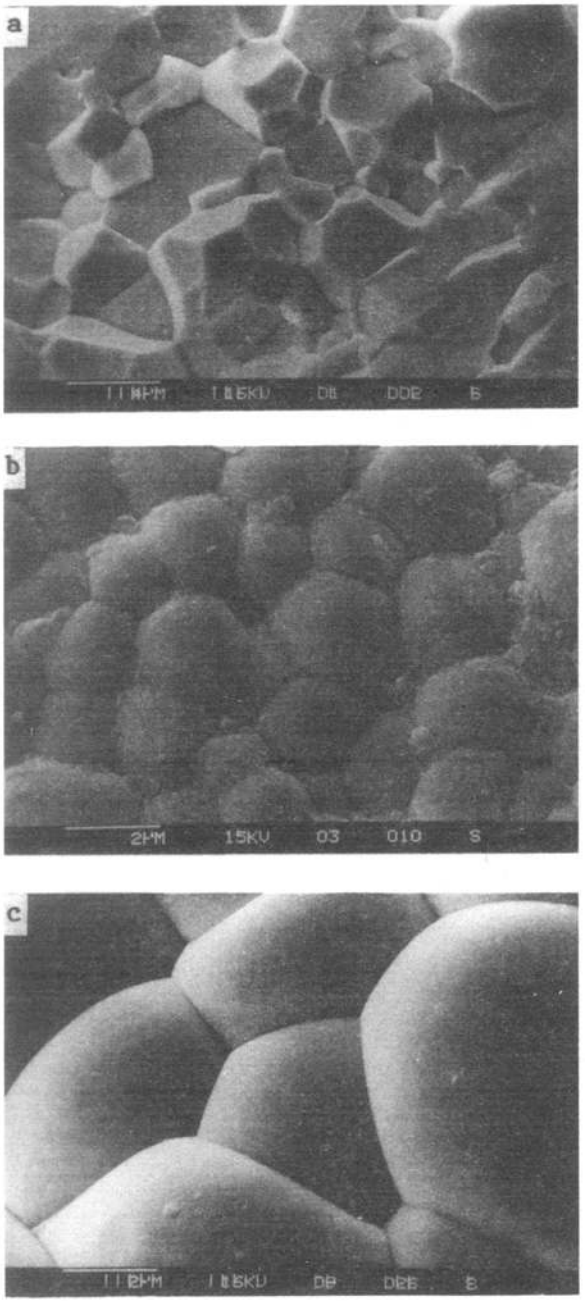

Figure 3. a–c.

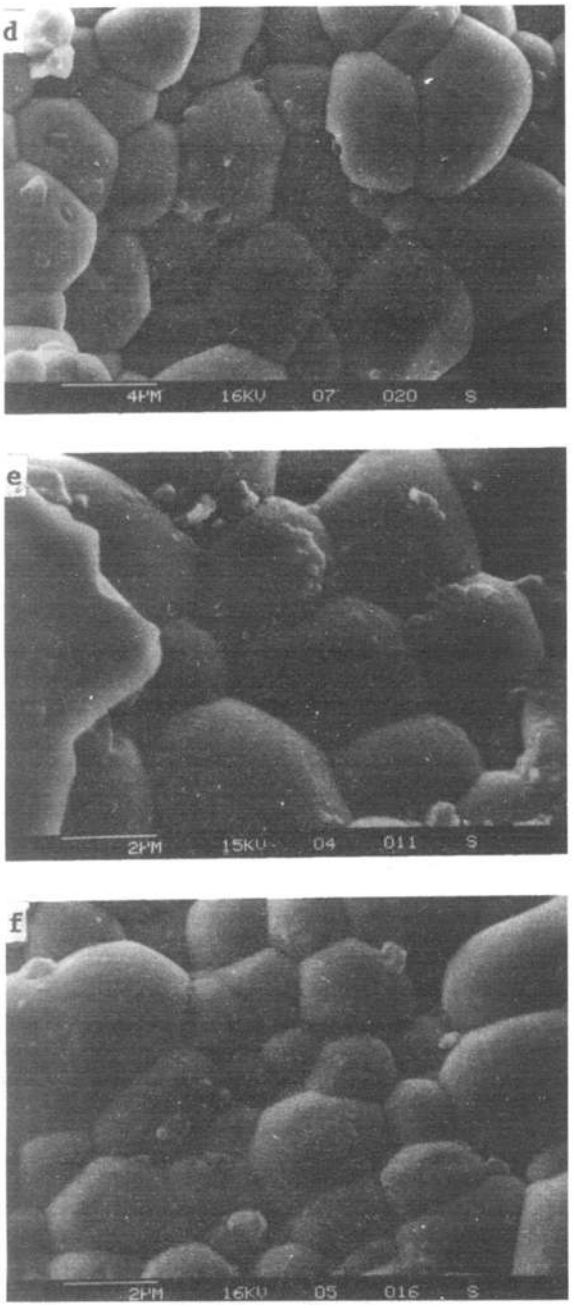

Figure 3. SEM photographs of fractured surface of (**a**) PMT2, (**b**) PMZN1, (**c**) PMZN2, (**d**) PMFN2, (**e**) PMZNT2 and (**f**) PMFNT2.

The samples PMT1, PMT2, PMZN1, PMZN2, PMZNT1 and PMZNT2 clearly exhibit a typical relaxor behaviour (figure 4). Increase in frequency decreases the magnitude of ε_{max} on one hand and increases $\tan\delta_{max}$ on the other and shifts the maxima in ε and $\tan\delta$ towards higher temperature. The $\tan\delta_{max}$ appears at a

Table 3. Grain size of perovskite phase and densification of PMN based solid solutions.

Sample	Grain size (μm)	Densification (%)
PMT1	2·1 ± 0·2	94
PMT2	4·9 ± 0·2	98
PMZN1	2·9 ± 0·2	95
PMZN2	6·9 ± 0·6	96
PMFN1	2·2 ± 0·2	93
PMFN2	6·6 ± 0·3	97
PMZNT1	–	95
PMZNT2	4·4 ± 0·3	97
PMFNT1	1·2 ± 0·3	93
PMFNT2	3·5 ± 0·4	97

temperature range lower than that corresponding to ε_{max}, indicating low losses near ambient temperature. The samples PMFN1, PMFN2, PMFNT1 and PMFNT2 show a systematic frequency dispersion in ε_{max} with temperature except the missing transition at 100 Hz in case of PMFN2 (figure 5). In contrast, no systematic variation of tanδ with temperature and frequency is observed, reflecting a deviation from the relaxor behaviour. The deviation from relaxor behaviour is found to be more pronounced for higher concentration of Fe and sintering temperature (figure 5). Low losses comparable to PMN are observed in case of PMT1, PMT2, PMZN1, PMZN2, PMZNT1, PMZNT2 and PMFNT1 samples. Whereas, slightly higher losses in PMFNT2 and substantially high losses are detected in PMFN1 and PMFN2 samples.

It is well known that in relaxors, there exists inbuilt compositional microinhomogeneity amongst individual unit cells. Such a microinhomogeneity results into a small variation in the potential energy of ferroactive B-site atoms of oxygen octahedra responsible for temperature sensitive atomic displacement and variation in relaxation time. A statistical average of identical compositional unit cells which have a transition temperature with a fixed relaxation time. Likewise, there could be different groups corresponding to similar compositions having same relaxation time. Therefore, with the change in frequency, T_c changes as each will have different relaxation frequency as reflected in figure 4. Anologously inbuilt heterogeneity in compositions within unit cell to unit cell results into variation in soft modes that spreads over the temperature region giving rise to DPT behaviour.

For all compositions it is seen that an increase in sintering temperature (table 4) increases the permittivity maximum but lowers the transition temperature. A closer look at table 4 reveals that PMZNT1 (sintered at 1080°C) and PMZNT2 (sintered at 1180°C) exhibit highest permittivity maximum equal to 19740 and 23700 respectively. It is worth noting here that PMZNT1 ($T_c = 34·5$°C) gave almost same value of permittivity maximum as that of PMN ($T_c = -16$°C) sintered at 1200°C (Wang and Schulze 1990). Interestingly, the permittivity maximum obtained in PMT2 is found to be comparable with that of reported permittivity maximum = 20372 for gel derived ceramics (Ravindranathan *et al* 1991). Also, the permittivity maximum obtained in PMZN1 is observed to be significantly higher than the reported value of the order 14400 (Landin and Schulze 1990). On the other hand 0·9PMN–0·1PT and 0·85PMN–0·07PFN–0·08PT exhibit reasonably high permittivity maximum provided they are sintered at higher temperature ($\geq$ 1150°C) (table 4).

Table 4. ε_{max}, T_c, $\tan\delta_{max}$ and $T\tan\delta_{max}$ of PMN based solid solutions at 0·1, 1, 10 and 100 kHz.

	100 Hz				1 kHz				10 kHz				100 kHz	
Sample	ε_{max}	T_c (°C)	$\tan\delta_{max}$	$T\tan\delta_{max}$ (°C)	ε_{max}	T_c (°C)	$\tan\delta_{max}$	$T\tan\delta_{max}$ (°C)	ε_{max}	T_c (°C)	$\tan\delta_{max}$	$T\tan\delta_{max}$ (°C)	ε_{max}	T_c (°C)	$\tan\delta_{max}$	$T\tan\delta_{max}$ (°C)
PMT1	12000	42·5	0·0510	26	11390	45	0·0566	28	10820	48	0·0650	30	10240	51·5	0·0780	33
PMT2	21660	37	0·0910	22	19680	39·5	0·0975	24	17920	42	0·1110	26·5	16400	45	0·1250	28·5
PMZN1	17060	27·5	0·0950	14	15730	30	0·1020	16·5	14480	33·5	0·1130	19	13290	37·5	0·1280	22
PMZN2	18270	24	0·0937	12·5	17270	26·5	0·1030	14·5	16110	30	0·1150	17	15130	35	0·1377	20·5
PMFN1	11000	24	—	—	10700	26	—	—	10200	28	—	—	9600	30	—	—
PMFN2	—	—	—	—	19000	20	—	—	16170	23·5	—	—	14460	27	—	—
PMZNT1	19740	34·5	0·0830	20·5	18260	37·5	0·0884	22·5	16850	40·5	0·1006	24·5	15550	44	0·1140	27
PMZNT2	23700	33·5	0·0910	20	21820	36·5	0·0980	22	19980	39·5	0·1100	24	18230	43	0·1300	26·5
PMFNT1	9800	32·5	0·1220	20	9100	35	0·0875	21	8700	38	0·0815	23	8300	41	0·0877	24
PMFNT2	22840	29·5	0·1550	20	19900	32·5	0·1295	21·5	17530	35·5	0·1180	23	15790	38·5	0·1250	25

$\tan\delta_{max}$ → Maximum value of dissipation factor; $T\tan\delta_{max}$ → Temperature corresponding to $\tan\delta_{max}$.

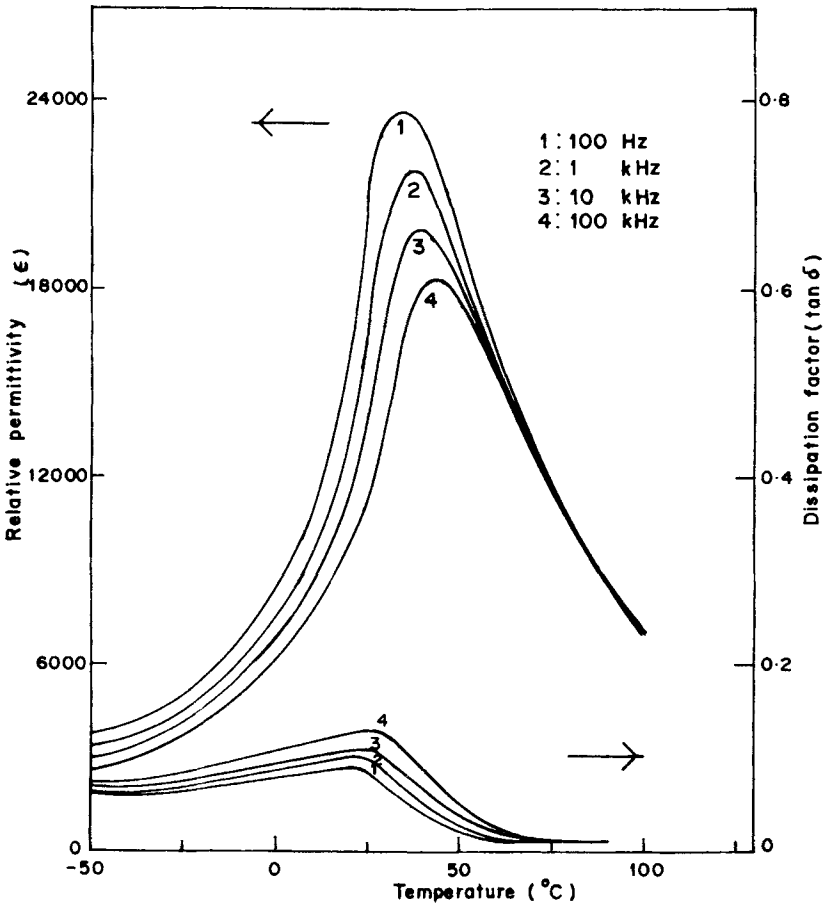

Figure 4. Temperature dependence of relative permittivity (ε) and dissipation factor ($\tan\delta$) of PMZNT2 at 0·1, 1, 10 and 100 kHz.

As stated earlier our interest was in developing the relaxors with high permittivity and T_c near room temperature. Hence the compositions have been selected for the present study wherein, T_c ranged within 24 to 42·5°C at Hz (table 4).

The highest permittivity maximum obtained for PMZNT2 is apparently due to improved perovskite phase, higher density and high intrinsic permittivity of PZN. In PMFN2, the anamoly in high permittivity seems to be a result of space charge polarization arising due to oxygen vacancies during sintering process leading to partial conversion of Fe^{3+} to Fe^{2+} in the interfaces of the grain boundaries. The Fe^{3+} to Fe^{2+} conversion is supported with the naked eye observation of the change in colour from brown to black seen in cases of PMFN1 and PMFN2. The above results are in total agreement with the suggested model (Ichinose and Kato 1994; Yokosuka 1995). Hence in conclusion, the increase in Fe concentration and sintering temperature together promote the conversion of Fe^{3+} to Fe^{2+} leading to increase in ε and high losses. The quadratic law,

$$\frac{1}{\varepsilon}=\frac{1}{\varepsilon_{max}}+(T-T_c)^2/2\varepsilon_{max}\delta^2, \tag{2}$$

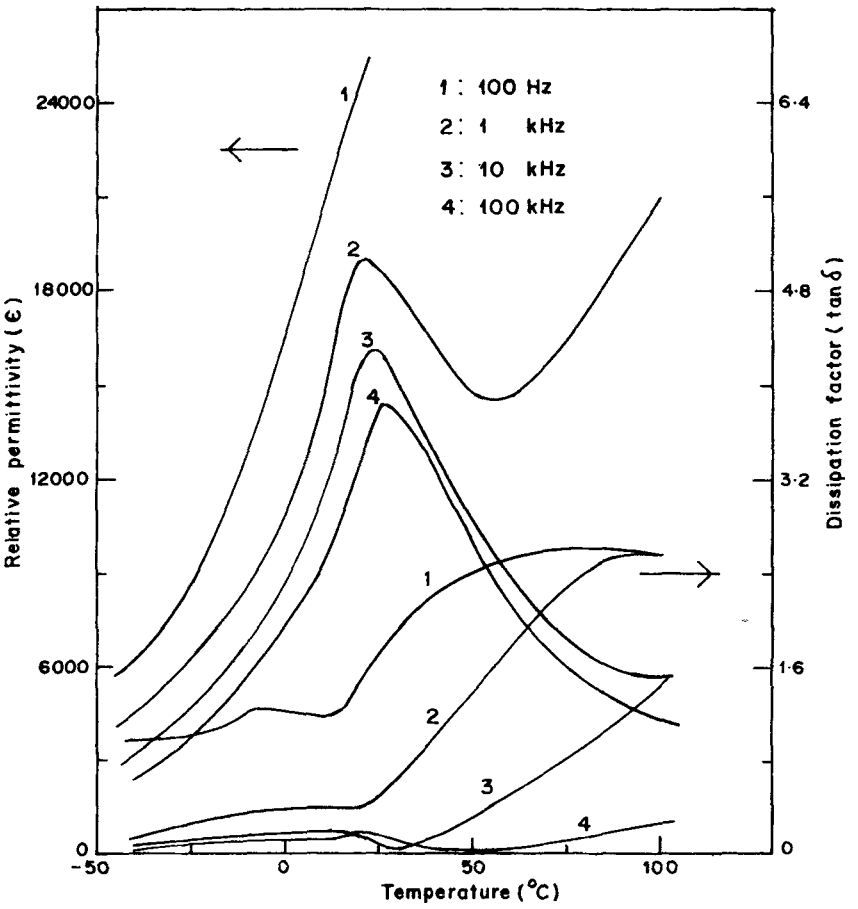

Figure 5. Temperature dependence of relative permittivity (ε) and dissipation factor ($\tan\delta$) of PMFN2 at 0·1, 1, 10 and 100 kHz.

where, T and δ are temperature above T_c and diffusion coefficient respectively established for DPT materials is found to be valid over a temperature range of investigation for all samples except PMFN1 and PMFN2.

The plots of $1/\varepsilon$ vs $(T-T_c)^2$ for PMFN1, PMFN2 and PMZNT1, PMZNT2 samples are depicted in figures 6a–d respectively. The large deviation from linearity is observed with increased concentration of Fe at higher sintering temperature (figure 6b). The diffusion coefficient calculated using (2) at 1 kHz along with the difference between transition temperature ΔT_c measured at 0·1 to 100 kHz i.e. curie range, are presented in table 5. The general trend of decrease in diffusion coefficient with increase in permittivity maximum is observed in case of 0·9PMN–0·1PT and 0·85PMN–0·07PFN–0·08PT solid solutions. However 0·7PMN–0·3PZN shows opposite behaviour, whereas, no detectable change is observed in case of 0·85PMN–0·07PZN–0·08PT solid solution.

3.3 *Sintered density and dc resistivity*

The values of sintered density of all the samples are presented in table 3. As expected, higher density is achieved in all compositions of solid solution sintered at higher

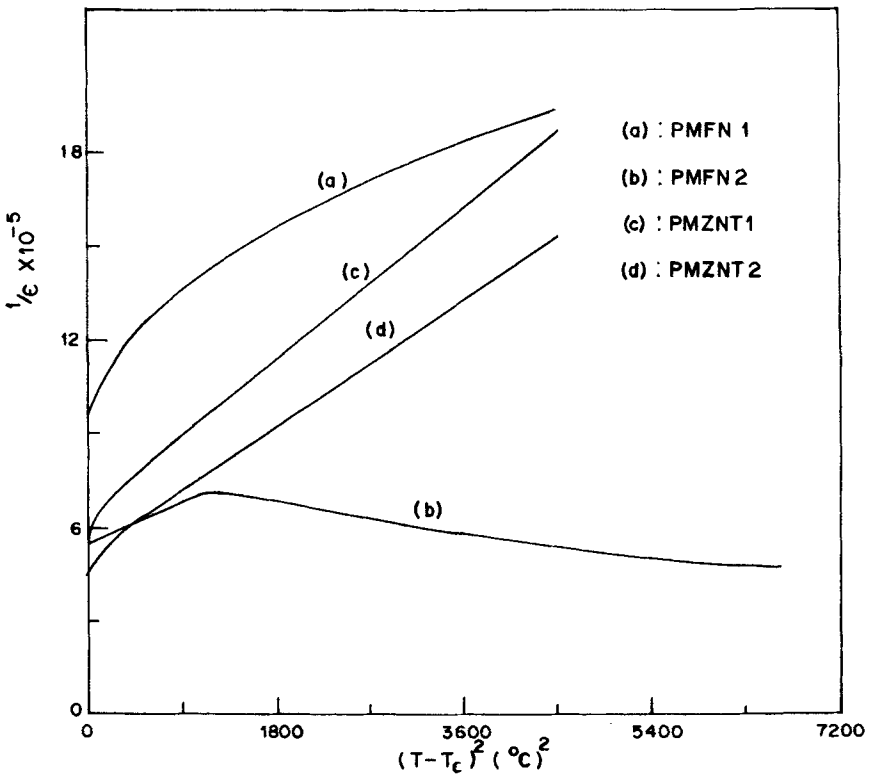

Figure 6. Plots of reciprocal of relative permittivity $1/\varepsilon$ vs $(T-T_c)^2$ at 1kHz for (a) PMFN1, (b) PMFN2, (c) PMZNT1 and (d) PMZNT2.

Table 5. Diffusion coefficient (δ) and curie range (ΔT_c) of PMN based solid solutions.

Sample	δ (°C)	ΔT_c (°C)
PMT1	45	9
PMT2	37	8
PMZN1	35	10
PMZN2	41	11
PMZNT1	32	9·5
PMZNT2	32	9·5
PMFNT1	55	9
PMFNT2	33	8·5

temperature. It is worth noting that 95 % of theoretical density is obtained for PMZN1 and PMZNT1 samples inspite of sintering at low temperature (1080°C). Furthermore, 96 % density obtained for PMZN2 sintered at 1180°C indicates attainment of saturation in density in case of 0·7PMN–0·3PZN solid solution. These results are similar to those of Landin and Schulze (1990). A relatively lower density (96 %) obtained for PMZN2 is a consequence of higher content of low density pyrochlore phase present therein.

In general, the d.c. resistivity at room temperature is found to be $\geqslant 10^{12}$ ohm-cm except for PMFN1, PMFN2 and PMFNT2. However, PMFN1, PMFN2 and PMFNT2 shows resistivity of the order of 10^7, 10^5 and 10^8 ohm-cm respectively. Voss *et al* (1983), also reported low resistivity in case of Fe doped PMN. The rapid fall in resistivity in Fe containing samples, for increasing Fe content and sintering temperature, is due to the increased oxygen vacancies leading to ionic conduction. Similar effect has also been observed by Yokosuka (1995).

4. Conclusions

All the compositions selected in the present study form solid solution with PMN. ZnO addition in PMN as well as in PMN–PT improves sinterability. A fairly high relative permittivity maximum obtained for PMZN1 with $T_c = 27{\cdot}5°C$ and PMZNT1 with $T_c = 34{\cdot}5°C$ reflected low firing capabilities of these relaxors satisfying the present demand for practical utilization. In contrast, Fe associated solid solutions exhibit high permittivity accompanied with high losses which limit their practical utility.

References

Bokov V A and Mylnikova I E 1961 *Sov. Phys. Solid State* **2** 2428
Bouquin O and Lejeune M 1991 *J. Am. Ceram. Soc.* **74** 1152
Desgardin G, Bali H and Raveau B 1983 *Mater. Chem. & Phys.* **8** 469
Goldschmidt V M 1926 *Shrifter Norske Videnskaps-Akad. Oslo: Matemot. Naturuid. Klasse*, No 2
Ichionse K and Kato N 1994 *J. Appl. Phys.* **33** 5423
Landin S M and Schulze W A 1990 *J. Am. Ceram. Soc.* **73** 913
Lejeune M and Boilot J P 1985 *Mater. Res. Bull.* **20** 493
Ravindranathan P, Komarneni S, Bhalla A and Roy R 1991 *J. Am. Ceram. Soc.* **74** 2996
Shrout T R and Halliyal A 1987 *Am. Ceram. Soc. Bull.* **66** 704
Singh K and Band S A 1996 *Ferroelectrics* **175** 193
Smolenskii G A and Agranovskaya A I 1959 *Sov. Phys. Solid State* **1** 1429
Swartz S L and Shrout T R 1982 *Mater. Res. Bull.* **17** 1245
Swartz S L, Shrout T R, Schulze W A and Cross L E 1984 *J. Am. Ceram. Soc.* **167** 311
Voss D J, Swartz S L and Shrout T R 1983 *Ferroelectrics* **50** 203
Wang H C and Schulze W A 1990 *J. Am. Ceram. Soc.* **73** 825
Yan M F, Ling H C and Rhodes W 1989 *J. Mater. Res.* **4** 930
Yokosuka M 1995 *Jpn J. Appl. Phys.* **34** 5338